

Highly efficient MRI through multi-shot echo planar imaging

Congyu Liao^{a,b}, Xiaozhi Cao^c, Jaejin Cho^{a,b}, Zijing Zhang^{a,d}, Kawin Setsompop^{a,b}, Berkin Bilgic^{*a,b}

^aAthinoula A. Martinos Center for Biomedical Imaging, Massachusetts General Hospital, Charlestown, MA, USA; ^bDepartment of Radiology, Harvard Medical School, Boston, MA, USA;

^cCenter for Brain Imaging Science and Technology, Zhejiang University, Hangzhou, China;

^dThe State Key Laboratory of Modern Optical Instrumentation, College of Optical Science and Engineering, Zhejiang University, Hangzhou, China

ABSTRACT

Multi-shot echo planar imaging (msEPI) is a promising approach to achieve high in-plane resolution with high sampling efficiency and low T_2^* blurring. However, due to the geometric distortion, shot-to-shot phase variations and potential subject motion, msEPI continues to be a challenge in MRI. In this work, we introduce acquisition and reconstruction strategies for robust, high-quality msEPI without phase navigators. We propose Blip Up-Down Acquisition (BUDA) using interleaved blip-up and -down phase encoding, and incorporate B_0 forward-modeling into Hankel structured low-rank model to enable distortion- and navigator-free msEPI. We improve the acquisition efficiency and reconstruction quality by incorporating simultaneous multi-slice acquisition and virtual-coil reconstruction into the BUDA technique. We further combine BUDA with the novel RF-encoded gSlider acquisition, dubbed “BUDA-gSlider”, to achieve rapid high isotropic-resolution MRI. Deploying BUDA-gSlider with model-based reconstruction allows for distortion-free whole-brain 1mm isotropic T_2 mapping in ~ 1 minute. It also provides whole-brain 1mm isotropic diffusion imaging with high geometric fidelity and SNR efficiency. We finally incorporate sinusoidal “wave” gradients during the EPI readout to better use coil sensitivity encoding with controlled aliasing.

Keywords: MRI; multi-shot EPI; distortion-free EPI; low-rank reconstruction; diffusion MRI; T_2 map; wave-EPI.

1. INTRODUCTION

Echo planar imaging (EPI) is an efficient acquisition technique for fast MRI. The single-shot variant of EPI (ssEPI) which acquires the entire k-space data in a single TR is the most commonly used approach, for its fast acquisition and its immunity to bulk motion. However, the associated lengthy echo train of ssEPI induces T_2^* blurring and geometric distortion, imposing a limitation on the achievable resolution. Multi-shot EPI (msEPI) allows high-resolution imaging with reduced distortion, but combining shots is prohibitively difficult because of shot-to-shot phase variations. These variations can be mitigated using navigators^{1,2}, albeit at the cost of imaging efficiency and potential remaining artifacts. Navigator-free approaches^{3–5} employ parallel imaging (PI)^{6,7} to reconstruct each shot, from which phase variations are estimated. This imposes a limit on the distortion reduction since PI breaks down beyond $R_{\text{inplane}} > 4$ acceleration.

Recently, Hankel structured low-rank constrained PI approaches^{8–12} were proposed to enable navigator-free msEPI acquisition with higher in-plane acceleration to minimize geometric distortion. However, achieving adequate image quality at higher acceleration necessitates a larger number of shots (e.g., $R_{\text{inplane}}=8$ with 4-shots), thereby limiting the efficiency of such acquisitions. In previous work^{13–15}, we incorporated virtual coil (VC) concept¹⁶ and simultaneous multi-slice (SMS) acquisition^{17,18} into structured low-rank model and deep learning-based reconstructions to further accelerate msEPI. Similar works were reported by other groups^{19,20}.

In this study, we propose an efficient Blip Up-Down Acquisition (BUDA), where a 2-shot EPI sampling was performed with interleaved blip-up and -down acquisitions, and then combined with B_0 forward-modeling and structured low-rank reconstruction to yield distortion-free images. With BUDA, the required number of shots was reduced to two, which improved the sampling efficiency of msEPI. We demonstrate its extension to the VC concept through structured low-rank reconstruction and obtain high-quality images from a partial Fourier 75% acquisition. We further combine BUDA with a

* BBILGIC@mgh.harvard.edu

novel volumetric RF-encoding technique, dubbed generalized slice dithered enhanced resolution (gSlider) acquisition²¹, to enable high signal-to-noise ratio (SNR) efficiency, high isotropic-resolution imaging with high geometric fidelity. Finally, we apply our proposed BUDA-gSlider to encoding-intensive diffusion-weighted imaging (DWI) and quantitative T₂ mapping, to achieve rapid whole-brain 1mm isotropic DWI and T₂ maps without geometric distortion. In addition, we demonstrate that employing sinusoidal “wave” gradients during the EPI readout improves image quality by better harnessing coil sensitivity encoding.

2. METHODS

2.1 Multi-shot EPI with Blip Up-Down Acquisition (BUDA)

Figure 1(a) shows the sampling strategy of a two-shot BUDA acquisition, where two interleaved shots with blip-up and -down phase encoding polarity were collected. Figure 1(b) shows the flowchart of BUDA reconstruction, which includes the following steps: (i) individual SENSE reconstructions for blip-up and blip-down acquisitions, respectively. As blue arrows pointed in Figure 1(b), each individual shot has significant geometric distortion along the phase-encoding direction. (ii) Estimating the field maps using SENSE reconstructed blip-up and blip-down images. The field maps are estimated using FSL TOPUP^{22,23}. (iii) Incorporating field map forward-modeling into Hankel structured low-rank constrained joint reconstruction, which can be expressed as:

$$\min_x \sum_{t=1}^{N_s} \|F_t E_t C x_t - d_t\|_2^2 + \lambda \|\mathcal{H}(x)\|_*, \quad (1)$$

where F_t is the undersampled Fourier operator in t^{th} shot, E_t is the estimated off-resonance information, C are the ESPIRiT coil sensitivities²⁴ estimated from a distortion-free gradient-echo prescan data, x_t is the distortion-free image and d_t are the k-space data for shot t . In the forward model, the distortion-free images are multiplied by coil sensitivities and distorted by the phase modulation of the off-resonance map in hybrid (x-k_y) space. The constraint $\|\mathcal{H}(x)\|_*$ enforces low-rank prior on the block-Hankel representation of the multi-shot data x , which is applied in k-space where 7x7 blocks of k-space are concatenated from each shot in the column axis.

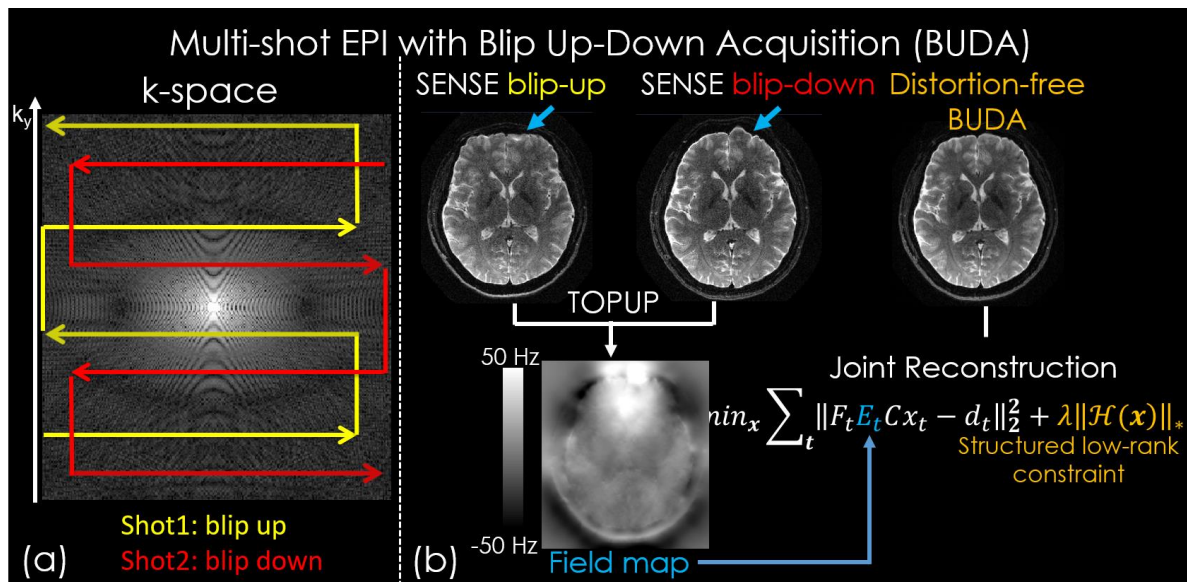


Figure 1. (a) two-shot EPI with blip up-down acquisition (BUDA) strategy. (b) The flowchart of BUDA reconstruction.

2.2 Joint virtual coil reconstruction for simultaneous multi-slice BUDA

The VC concept^{16,25} is an approach that utilizes smooth phase prior for reconstruction. The virtual coils containing conjugate symmetric k-space signals are generated from actual coils, which effectively doubles the number available channels. These allow for incorporating additional phase information into standard SENSE⁶ or GRAPPA⁷ to improve the reconstruction performance in a number of applications^{15,25–28}. In particular, our previous studies^{10,14,15} have demonstrated

that the VC reconstruction can provide improved SNR with reduced g-factor in diffusion-weighted spin-echo and spin-and-gradient echo (SAGE) EPI acquisitions. With VC reconstruction, Eq. (1) can be modified as:

$$\min_m \sum_{t=1}^{N_s} \left\| \begin{bmatrix} F_t E_t C \\ F_{-t} E_t C^* \end{bmatrix} x_t - \begin{bmatrix} d_t \\ d_{-t}^* \end{bmatrix} \right\|_2^2 + \lambda \| \mathcal{H}(x) \|_* \quad (2)$$

Here, d_{-t}^* is the VC k-space, and C^* are the corresponding conjugate sensitivities. Figure 2 shows the flowchart of the proposed joint VC reconstruction, where the conjugate shots are incorporated into the Hankel low-rank matrix, whereby the sampled conjugate-symmetric k-space helps estimate the missing data and substantially improves the reconstruction. To better take advantage of the conjugate property of k-space, a shifted- k_y EPI sampling strategy¹⁴ (Δk_y shift =1 for the blip-up shot and Δk_y shift =3 for the blip-down shot at $R_{\text{inplane}}=4$) was used to provide g-factor improvement over a non-shifted symmetric undersampling.

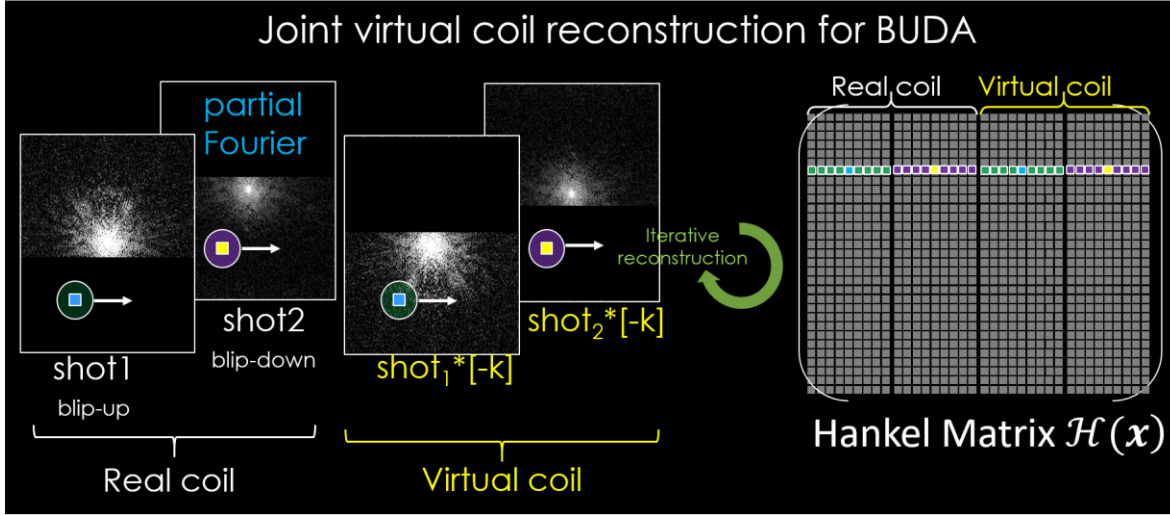


Figure 2. The flowchart of joint virtual coil reconstruction for BUDA. Virtual coils provide complementary k-space information in the presence of partial Fourier undersampling.

We further extended our VC-BUDA to simultaneous multi-slice (SMS) acquisition. Our previous work²⁹ developed an approach to allow structured low-rank constrained reconstruction to work with SMS encoding using the readout-extended FOV concept. This represents SMS as undersampling in the k_x axis by concatenating the two slices along the readout direction. In-plane and slice acceleration could thus be captured using the Fourier operator F_t in Eq. (1), now with simultaneous k_x - k_y undersampling, which allowed us to further push the total acceleration and reduce TR for msEPI.

All in vivo measurements were performed on a 3T scanner (MAGNETOM Prisma, Siemens Healthineers, Erlangen, Germany). To validate the proposed VC-BUDA reconstruction, whole-brain $1.0 \times 1.0 \times 3 \text{ mm}^3$ resolution SE-EPI data were acquired using a 32-channel head array with TE/TR=56/2700ms. 2-shots were collected at multi-band factor=2, $R_{\text{inplane}}=4$ and partial Fourier (PF) 75%. The field-of-view (FOV) of EPI acquisition is 220 mm. A FOV-matched gradient-echo (GRE) sequence was acquired to obtain distortion-free sensitivity maps for BUDA reconstruction. A fast spin-echo (FSE) data was acquired to serve as a distortion-free reference. To demonstrate the utility of our proposed method, BUDA was compared with hybrid-SENSE⁵¹ on the same dataset.

2.3 Combining BUDA with RF-encoding acquisition (BUDA-gSlider) for diffusion imaging

BUDA provides a robust acquisition and reconstruction framework to achieve distortion-free high in-plane resolution MRI. To achieve high isotropic-resolution MRI with thin slices, improving the SNR efficiency of EPI acquisition is critical, especially in SNR-starved applications such as diffusion-weighted imaging (DWI). Three dimensional multi-slab diffusion-weighted EPI has emerged as a promising strategy to enhance the SNR in such acquisitions³⁰⁻³². However, slab-boundary artifacts are key challenges for efficient sampling of whole-brain high isotropic-resolution DWI with this technique^{33,34}. Another promising approach for high-SNR efficiency, high-resolution DWI is the Generalized SLice Dithered Enhanced Resolution (gSlider) method²¹. gSlider is a simultaneous multi-slab acquisition technique with self-

navigated RF slab-encoding, which has been demonstrated for motion-robust, high-resolution DWI³⁵. Here we combine BUDA and gSlider to achieve high geometric fidelity, high isotropic-resolution MRI without phase navigators.

Figure 3(a) shows the sequence diagram of the proposed BUDA-gSlider, where both blip-up and blip-down shots are acquired in each RF-encoding sequentially. Five RF-encoding pulses with the sharp sub-slice encoding performance shown in Figure 3(b) were designed by Shinnar-Le Roux (SLR) algorithm³⁶ and used for slab-encoding³⁷. With five gSlider RF-encoding pulses and 2 blip up-down shots, a total of $5 \times 2 = 10$ shots were acquired for each slab. These RF excitations were then combined with blipped-CAIPI technique (multiband factor of 2)¹⁸ to acquire 10 simultaneous slices per EPI-shot.

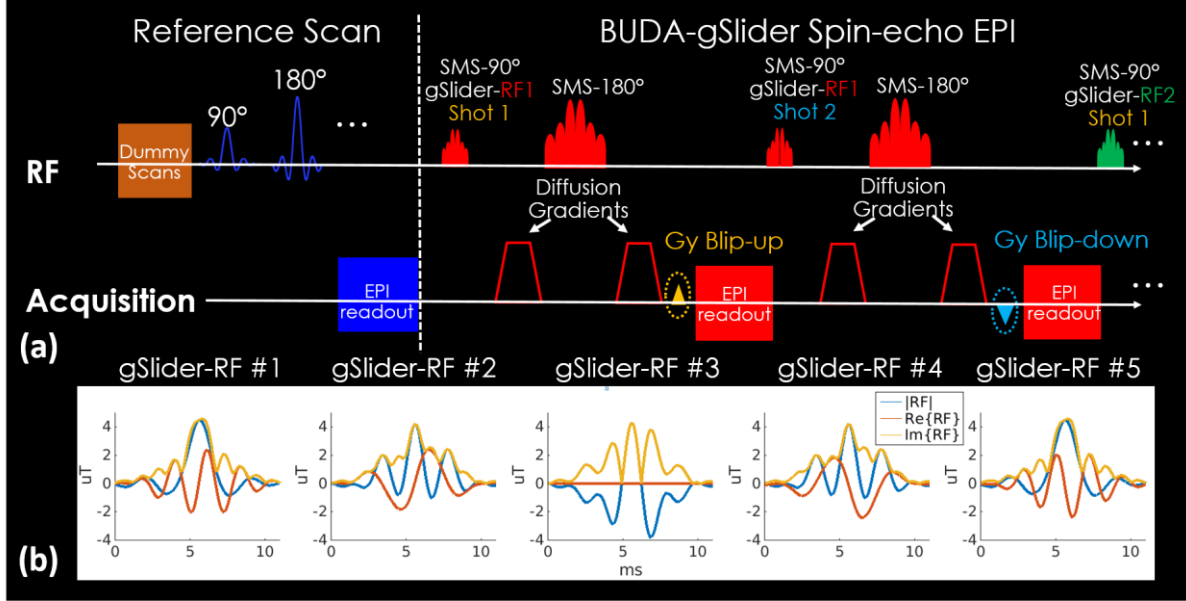


Figure 3. (a) The sequence diagram of BUDA-gSlider, where both blip-up and blip-down shots are acquired in each RF-encoding. (b) Five RF-encoded gSlider pulses used in the BUDA-gSlider sequence. 5x-gSlider with slice phase-dither encoding provides highly independent basis, while maintaining high image SNR in each individual slab acquisition.

The reconstruction of BUDA-gSlider data includes the following steps: (i) SMS-BUDA reconstruction was performed for each RF encoding to obtain distortion-free thin-slab volume. (ii) To eliminate shot-to-shot background phase variations in the acquired gSlider data, real-valued diffusion processing³⁸ was applied to each RF-encoded volume. (iii) gSlider reconstruction was then performed to obtain high slice-resolution data, using a forward model based on the Bloch simulated slab profiles of the gSlider encodings, which can be expressed as:

$$\mathbf{X} = (\mathbf{A}^T \mathbf{A} + \lambda \mathbf{I})^{-1} \mathbf{A}^T \mathbf{b}, \quad (3)$$

where \mathbf{b} is the concatenation of acquired thin-slab data at a given in-plane spatial location, \mathbf{X} is the corresponding super-resolution reconstruction, \mathbf{A} is the RF-encoding matrix that contains the sub-slab profiles simulated from the Bloch equations and λ is a Tikhonov regularization parameter. To reduce slab-boundary artifacts of super-resolution images, B_1^+ and T_1 corrections³⁹ were incorporated into the gSlider reconstructions. After these steps, the reconstructed high slice-resolution images were used for further image analysis.

To this end, whole-brain 1 mm isotropic resolution diffusion imaging data were acquired with BUDA-gSlider-EPI. The protocol used: $\text{FOV} = 220 \times 220 \times 130 \text{ mm}^3$, $R_{\text{inplane}} \times \text{gSlider} = 4 \times 5$, 26 thin-slabs (5 mm slab-encoding), $b = 1000 \text{ s/mm}^2$ with 64 diffusion-directions and 4 interleaved $b = 0 \text{ s/mm}^2$, $\text{TR/TE} = 3500/86 \text{ ms}$. The total acquisition time is ~40 minutes. A matching T_2 weighted 3D-FSE data was acquired to serve as a distortion-free reference.

The virtual-coil BUDA and gSlider reconstruction algorithms were implemented in MATLAB R2014a (The MathWorks, Inc., Natick, MA). The reconstructed data were then corrected for motion and eddy-current distortion using the “eddy” function from the FMRIB Software Library²² (FSL, <https://fsl.fmrib.ox.ac.uk/fsl/fslwiki/>). Diffusion tensor model was fitted using FSL’s “dtifit” function to obtain fractional anisotropy (FA) maps and primary eigenvectors.

2.4 Fast T₂ mapping using BUDA-gSlider with echo-time shuffling

High isotropic-resolution T₂ mapping has great potential in clinical and neuroscience applications⁴⁰ but its acquisition is hindered by low SNR and long acquisition time. In spite of recent technical advances^{41–45}, rapid and robust acquisition remains a challenge for whole-brain high-resolution quantitative imaging. Based on the BUDA-gSlider acquisition, we propose a model-based reconstruction which combines shuffling algorithm⁴⁵ with different echo-time (TE) to achieve distortion-free high isotropic-resolution images with different T₂-weighted contrasts.

As shown in Figure 4(a), three out of five different TEs were acquired in each RF-encoded slab and were individually reconstructed by VC-BUDA. The sampled thin-slab images were then combined to expand along the RF-encoding-TE dimension of \mathbf{b}_{exp} and incorporated into our joint shuffling-gSlider model. By using the extended phase graph (EPG) algorithm⁴⁶, a dictionary with signal evolution curves of T₂'s from 1 to 1000 ms was built (temporal basis Φ shown in Figure 4b). Figure 4(c) shows our proposed reconstruction, where the joint gSlider-shuffling model reconstructs the super-resolution slice images and exploits the low-rank property by projecting the super-resolution images along the TE dimension to temporal basis simultaneously. The thin super-resolution temporal coefficient maps \mathbf{c}_{exp} can be obtained by solving:

$$\min_{\mathbf{c}_{\text{exp}}} \|\mathbf{b}_{\text{exp}} - \mathbf{A}_{\text{exp}} \Phi_{\text{exp}} \mathbf{c}_{\text{exp}}\|_2^2 + R(\mathbf{c}_{\text{exp}}), \quad (4)$$

where \mathbf{A}_{exp} is the expanded RF-encoding matrix, $R(\mathbf{c}_{\text{exp}})$ is the Tikhonov regularization and Φ_{exp} is the expanded temporal basis. The weak temporal coefficients (C3 to C5) were truncated using low-rank approximation. Thin-slice images with different T₂ contrast were recovered using $\Phi_{\text{exp}}^T \mathbf{c}_{\text{exp}}$ and matched to the pre-calculated dictionary to obtain the final T₂ maps (Figure 4c).

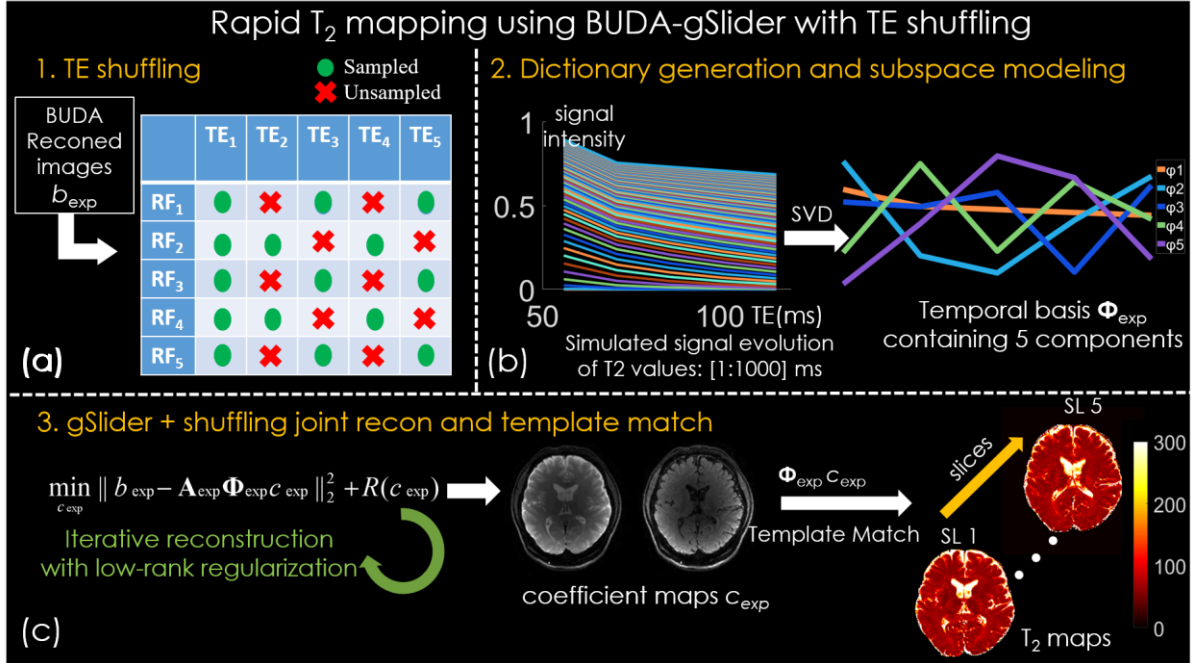


Figure 4. Reconstruction process including initialization with shuffled sampling pattern (a), dictionary generation (b), gSlider-Shuffling joint reconstruction and template match with a pre-calculated T₂ dictionary (c).

For rapid, high-quality T₂ mapping, the T₂ BUDA-gSlider with 2-shots at multi-band factor=2 and R_{inplane}=4 acceleration was acquired with 5 RF-encodings. The imaging parameters were: FOV= 220×220×130 mm³, 26 thin-slabs (slab-thickness=5mm), TR=2100 ms, 5 TEs=[56, 71, 86 101 and 116] ms. With TE-shuffling acquisition, only three out of five TEs were selected per each RF encoding. The shuffled sampling pattern is shown in Figure 5(a). The proposed T₂-gSlider enables high-quality whole-brain T₂ mapping with 1-mm isotropic resolution in 63 seconds. To assess the accuracy of the estimated T₂ maps from BUDA-gSlider, a single-echo spin-echo sequence with seven TEs were acquired as the gold

standard for comparison. The imaging protocol of single-echo spin-echo were: seven TEs=[25, 50, 75, 100, 125, 150, 200] ms, slice thickness =5 mm, in-plane resolution = $1 \times 1 \text{ mm}^2$, TR=3500 ms, total acquisition time = 30 minutes.

2.5 Multi-shot EPI with wave controlled aliasing in parallel imaging

Wave controlled aliasing in parallel imaging (wave-CAPI) employs extra sinusoidal gradient modulations during the readout to effectively use the coil sensitivity to achieve higher accelerations through parallel imaging^{47,48}. Herein, we demonstrate the application of wave-CAPI in EPI to provide higher in-plane acceleration and reduce B_0 -related distortion^{49,50}. We further combine wave-EPI with multi-shot acquisition to significantly reduce the effective echo-spacing time, and employ Hankel structured low-rank matrix completion to gain robustness against shot-to-shot phase variations.

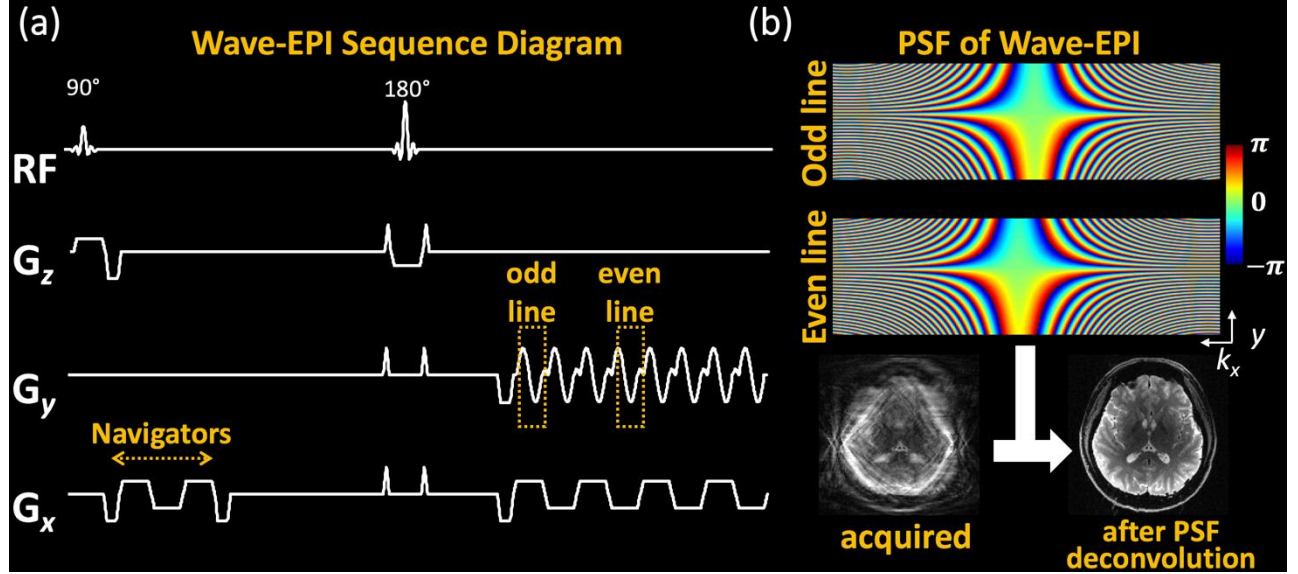


Figure 5. (a) EPI sequence diagram with wave-CAPI. The G_y gradient trajectory is time-reversed between even and odd lines to ensure that the same wave corkscrew is traced out in k -space lines with opposite polarities. (b) To account for the gradient timing differences, a separate PSF is used for the even and odd lines, where the delay along the readout (k_x) axis is visible. Last row demonstrates the application of PSF formalism to deconvolve the image spreading due to the sinusoidal gradients in wave-EPI and obtain a clean image.

Figure 5a shows the EPI sequence diagram with wave-CAPI. Due to eddy currents and system imperfections, the actual k -space trajectories as captured by a point spread function (PSF) formalism differ between the even and odd lines of wave-EPI as shown in Figure 5b. To mitigate shot-to-shot variations in wave-msEPI, we enhanced the low-rank property among multiple shots by truncating the singular values of the Hankel matrix as described in 2.1. Parallel imaging and separate even and odd PSF information are captured in a generalized SENSE forward model during the reconstruction.

To demonstrate preliminary results from wave-msEPI, we collected two acquisitions at $R_{\text{inplane}}=12$ -fold acceleration using 32 channel receiver and a single cycle of sine-wave gradient: (i) 4-shot EPI at $1 \times 1 \times 2 \text{ mm}^3$ voxels, FOV = $220 \times 220 \times 80 \text{ mm}^3$ using a maximum wave gradient amplitude 15 mT/m. (ii) 3-shot acquisition at $0.8 \times 0.8 \times 5 \text{ mm}^3$ voxels, FOV = $220 \times 220 \times 150 \text{ mm}^3$. The higher in-plane resolution and lower readout bandwidth of the second acquisition allowed for higher maximum gradient amplitude of 24 mT/m.

3. RESULTS

Figure 6 shows the hybrid-SENSE and VC reconstruction of a slice group of $1 \times 1 \times 3 \text{ mm}^3$ SMS-BUDA data at multiband $\times R_{\text{inplane}}=2 \times 4$ with partial Fourier 75% sampling. The results of individual SENSE reconstructions for blip-up and -down acquisitions show significant distortion despite $R_{\text{inplane}}=4$ acceleration. Compared to the individual SENSE, both hybrid-space SENSE and proposed VC-BUDA incorporate field maps into the forward model of the joint reconstruction to correct the geometric distortion. However, as the red arrows highlighted in Figure 6, the residual artifacts in the hybrid-SENSE reconstruction were eliminated in VC-BUDA, demonstrating that the proposed VC-BUDA has better reconstruction performance with reduced residual artifacts compared to the hybrid-SENSE.

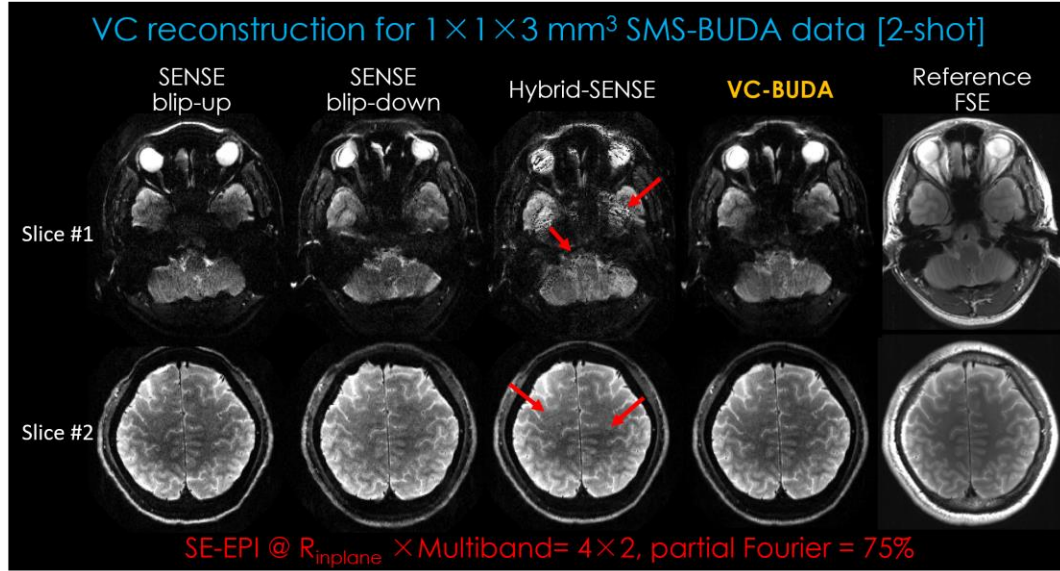


Figure 6. VC reconstruction for a slice-group of $1 \times 1 \times 3 \text{ mm}^3$ SMS-BUDA data. The VC-BUDA results were compared with hybrid-SENSE and reference FSE acquisition. The red arrows indicate the residual artifacts in the hybrid-SENSE reconstruction, which were eliminated in the VC-BUDA reconstruction.

Figure 7 compares image distortion between BUDA-gSlider and reference 3D-FSE images. The whole-brain 1mm isotropic diffusion volume reconstructed by the proposed BUDA-gSlider yielded images in three orthogonal views which closely matched those of the reference T_2 weighted 3D-FSE.

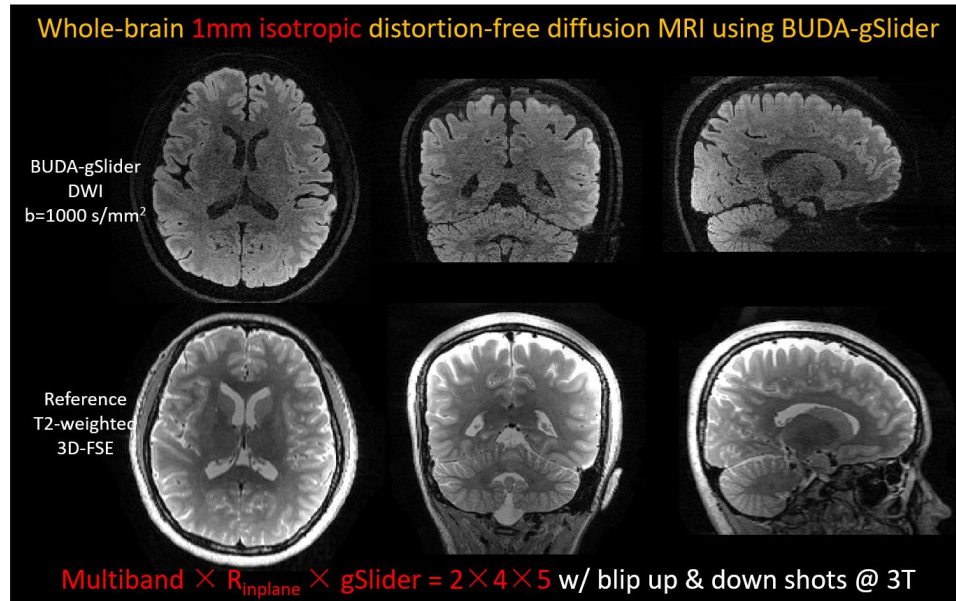


Figure 7. A 1mm-isotropic diffusion volume reconstructed by BUDA-gSlider method. The diffusion weighted volume retains very high geometric fidelity compared to the reference 3D-FSE images.

Figure 8 shows the averaged diffusion-weighted images from 64 diffusion-encoding directions and directionally-encoded color FA maps of the 1mm isotropic BUDA-gSlider diffusion data. BUDA-gSlider provides distortion-free diffusion images in the typically problematic frontal lobes, which are beneficial for mapping structural connectivity using diffusion tractography and mapping cortical diffusion patterns.

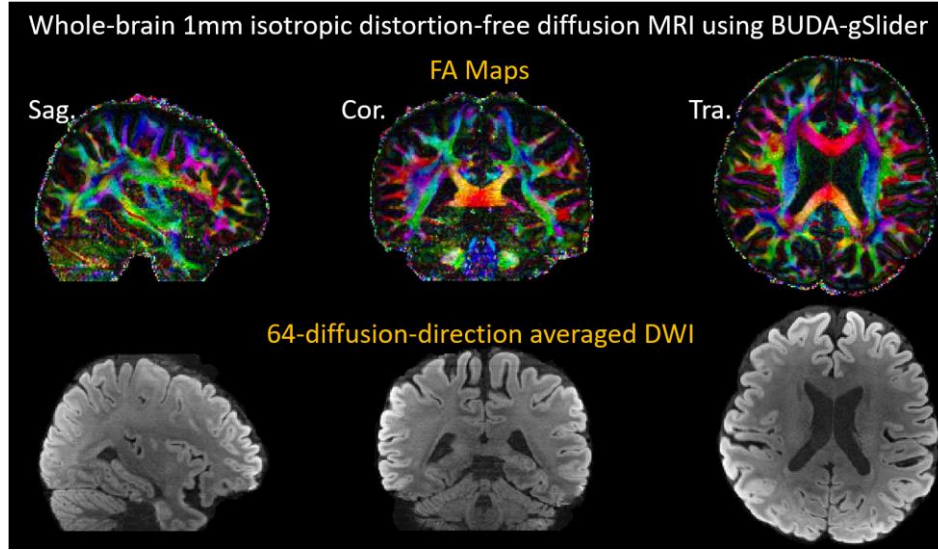


Figure 8. The FA and averaged diffusion-weighted images from 64-diffusion-direction whole-brain BUDA-gSlider data.

Figure 9 (a) shows whole-brain distortion-free T_2 maps from BUDA-gSlider with TE shuffling at 1mm^3 resolution, demonstrating high-quality whole-brain maps from a 1 minute acquisition. Figure 9 (b) compares the proposed T_2 BUDA-gSlider with the gold standard method. The bar plot shows the T_2 values estimated by T_2 BUDA-gSlider are very close to the gold standard in four represent regions but $\sim 30\times$ faster (60s vs 30 minutes), which demonstrate the utility of the proposed fast T_2 BUDA-gSlider.

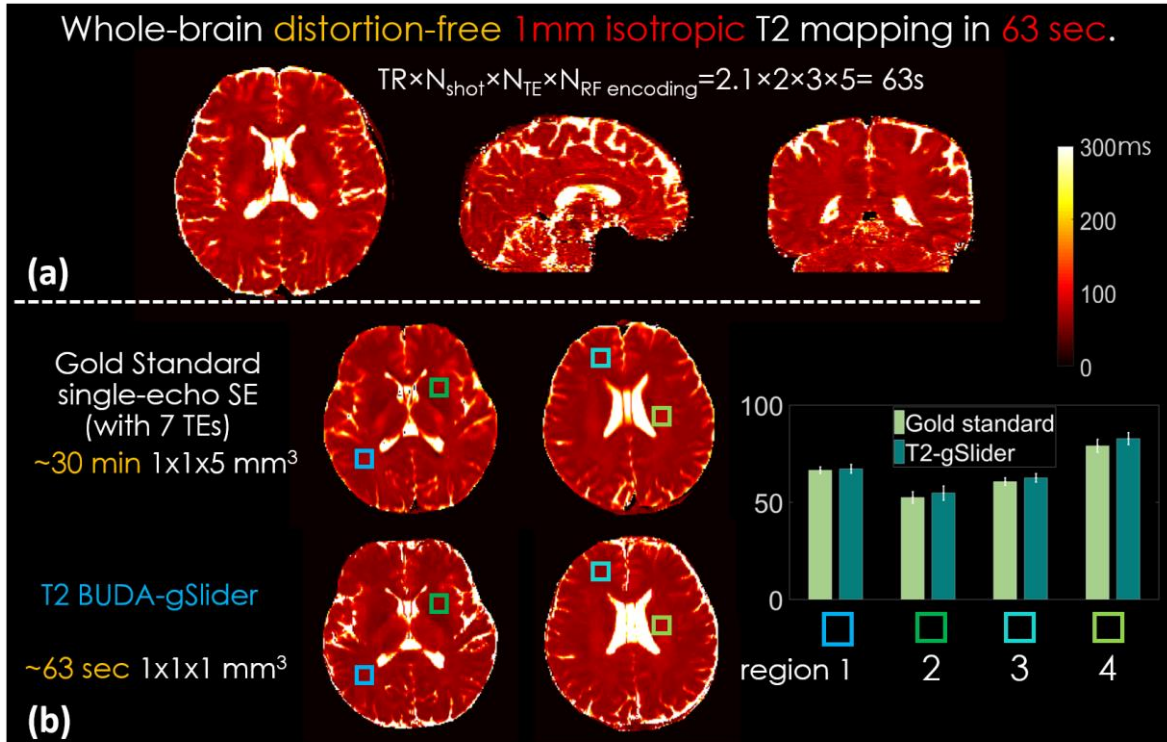


Figure 9. (a) T_2 maps in three views of 1-mm isotropic resolution with BUDA-gSlider acquisition with TE shuffling. (b) The comparison between T_2 BUDA-gSlider and gold standard method.

The preliminary results in Figure 10 demonstrate that the msEPI with wave-CAIPI could provide less aliasing artifacts (yellow arrows), less g-factor, and improved image quality compared to Cartesian msEPI. Specifically, wave-msEPI allowed for at least a 2-fold reduction in the maximum g-factor compared to the standard msEPI, and up to 30% improvement in the average g-factor metric.

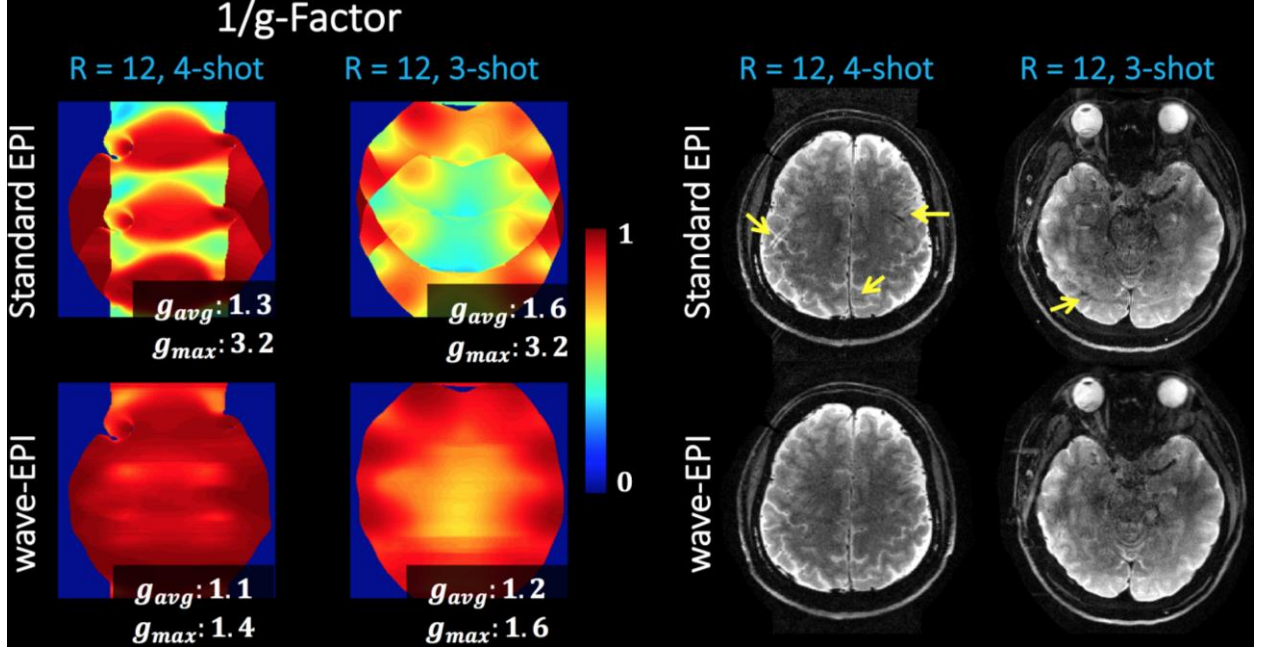


Figure 10. g-factor estimates and preliminary results for 3- and 4-shot msEPI acquisitions using standard Cartesian and wave-EPI. The yellow arrows highlight the aliasing artifacts of standard msEPI, while wave-EPI is able to mitigate the aliasing.

4. DISCUSSION

In this work, a highly efficient multi-shot EPI acquisition/reconstruction framework was proposed for rapid high isotropic-resolution, distortion-free structural, diffusion, and quantitative MRI. With interleaved blip up-down acquisition, the field maps were estimated and then incorporated into the forward model of reconstruction to obtain distortion-free images. To correct the shot-to-shot phase variations, Hankel structured low-rank constraint was used for multi-shot joint reconstruction. We also incorporated joint VC reconstruction and SMS concepts into BUDA reconstruction to push the limits of PF, in-plane and slice acceleration in the msEPI acquisition, and enabled high in-plane resolution, rapid structural imaging with high geometric fidelity. We further combine these methods with the gSlider acquisition to enable high SNR-efficiency, high isotropic-resolution imaging with enhanced SNR, which is beneficial for high fidelity diffusion imaging. In addition to diffusion acquisition, with TE-shuffling sampling strategy, BUDA-gSlider enables rapid whole-brain T_2 mapping with high isotropic resolution using SNR-efficient RF-encoded SE-EPI acquisition. Combined BUDA-gSlider reconstruction for in-plane undersampling with shuffling model for acceleration on RF-TE dimension, T_2 BUDA-gSlider can achieve high-quality, 1-mm isotropic whole-brain T_2 maps in ~ 1 minute without distortion. Additionally, employing wave gradients during the EPI readout could better harness sensitivity encoding to enable higher acceleration factors.

Previous studies such as hybrid-space SENSE⁵¹ performs joint reconstruction of the 2-shots by including their phase difference and field map into the forward model to correct both shot-to-shot phase variations and geometric distortion. However, due to the low SNR of diffusion-weighted images, it is difficult to estimate the phase difference accurately, which could cause residual artifacts and noise amplification. Our proposed BUDA exploits the Hankel low-rank model-based reconstruction, and obviates the need for phase-navigation or phase difference estimation by enforcing structured low-rank prior, which provides improved image quality and SNR. Furthermore, we incorporate VC concept into the BUDA framework to further improve the reconstruction performance using the conjugate symmetry property of k-space as prior

information, which is beneficial for partial Fourier reconstruction with complementary undersampling in blip-up and blip-down shots.

There are some limitations of BUDA method. Since BUDA requires an individual SENSE reconstruction for each shot to estimate the field map, inplane acceleration factor beyond 4-fold may fail to provide a robust reconstruction of individual shots. For high inplane resolution with a long EPI readout, the long T_2^* decay would cause image blurring at $R_{\text{inplane}}=4$. To address these issues, we are exploring wave-EPI as well as deep learning-based methods^{52,53} to achieve higher acceleration factor with robust reconstruction.

5. CONCLUSION

We proposed a multi-shot EPI based BUDA-gSlider acquisition/reconstruction strategy to provide high isotropic-resolution imaging without geometric distortion. We incorporated the virtual coil reconstruction and introduced wave-EPI to further improve the performance of image reconstruction. In vivo studies demonstrated that the proposed methods enabled high efficiency, high geometric fidelity multi-shot EPI for structural, diffusion weighted and quantitative imaging, which should provide high quality and efficiency MRI data in many clinical and neuroscientific applications.

6. ACKNOWLEDGEMENT

This work was supported in part by: National Institute of Biomedical Imaging and Bioengineering, Grant/Award Number: P41 EB015896, R01 EB017337, R01 EB019437, R01 EB020613 and U01 EB025162; National Institute of Neurological Disorders and Stroke, Grant/Award Number: K23 NS096056; National Institute of Mental Health, Grant/Award Number: R01 MH116173 and R24 MH106096; Center for Biomedical Imaging, Grant/Award Number: S10-RR023401 and S10-RR023043; NVIDIA GPU grant.

REFERENCES

- [1] Porter, D. A. and Heidemann, R. M., “High resolution diffusion-weighted imaging using readout-segmented echo-planar imaging, parallel imaging and a two-dimensional navigator-based reacquisition,” *Magnetic Resonance in Medicine* **62**(2), 468–475 (2009).
- [2] Jeong, H. K., Gore, J. C. and Anderson, A. W., “High-resolution human diffusion tensor imaging using 2-D navigated multishot SENSE EPI at 7 T,” *Magnetic Resonance in Medicine* **69**(3), 793–802 (2013).
- [3] Chen, N. Kuei, Guidon, A., Chang, H. C. and Song, A. W., “A robust multi-shot scan strategy for high-resolution diffusion weighted MRI enabled by multiplexed sensitivity-encoding (MUSE),” *NeuroImage* **72**, 41–47 (2013).
- [4] Guo, H., Ma, X., Zhang, Z., Zhang, B., Yuan, C. and Huang, F., “POCS-enhanced inherent correction of motion-induced phase errors (POCS-ICE) for high-resolution multishot diffusion MRI,” *Magnetic Resonance in Medicine* **75**(1), 169–180 (2016).
- [5] Liao, C., Chen, Y., Cao, X., Chen, S., He, H., Mani, M., Jacob, M., Magnotta, V. and Zhong, J., “Efficient parallel reconstruction for high resolution multishot spiral diffusion data with low rank constraint,” *Magnetic Resonance in Medicine* **77**(3), 1359–1366 (2017).
- [6] Pruessmann, K. P., Weiger, M., Scheidegger, M. B. and Boesiger, P., “SENSE: Sensitivity encoding for fast MRI,” *Magnetic Resonance in Medicine* **42**(5), 952–962 (1999).
- [7] Griswold, M. A., Jakob, P. M., Heidemann, R. M., Nittka, M., Jellus, V., Wang, J., Kiefer, B. and Haase, A., “Generalized Autocalibrating Partially Parallel Acquisitions (GRAPPA),” *Magnetic Resonance in Medicine* **47**(6), 1202–1210 (2002).
- [8] Haldar, J. P., “Low-Rank Modeling of Local k-Space Neighborhoods (LORAKS) for Constrained MRI,” *IEEE Transactions on Medical Imaging* **33**(3), 668–681 (2014).
- [9] Mani, M., Jacob, M., Kelley, D. and Magnotta, V., “Multi-shot sensitivity-encoded diffusion data recovery using structured low-rank matrix completion (MUSSELS),” *Magnetic Resonance in Medicine* **78**(2), 494–507 (2017).
- [10] Bilgic, B., Kim, T. H., Liao, C., Manhard, M. K., Wald, L. L., Haldar, J. P. and Setsompop, K., “Improving parallel imaging by jointly reconstructing multi-contrast data,” *Magnetic Resonance in Medicine* **80**(2), 619–632 (2018).

- [11] Lobos, R.A., Kim, T.H., Hoge, W.S. and Haldar, J.P., "Navigator-free EPI ghost correction with structured low-rank matrix models: New theory and methods," *IEEE transactions on medical imaging*, **37**(11), 2390-2402 (2018)
- [12] Shin, P. J., Larson, P. E. Z., Ohliger, M. A., Elad, M., Pauly, J. M., Vigneron, D. B. and Lustig, M., "Calibrationless parallel imaging reconstruction based on structured low-rank matrix completion," *Magnetic Resonance in Medicine* **72**(4), 959–970 (2014).
- [13] Bilgic, B., Liao, C., Manhard, M. K., Tian, Q., Chatnuntawe, I., Iyer, S. S., Cauley, S. F., Feiweier, T., Giri, S., Hu, Y., Huang, S. Y., Polimeni, J. R., Wald, L. L. and Setsompop, K., "Robust high-quality multi-shot EPI with low-rank prior and machine learning," *ISMRM*, 1250, Montreal, QC, Canada (2019).
- [14] Liao, C., Manhard, M. K., Bilgic, B., Tian, Q., Fan, Q., Han, S., Wang, F., Park, D. J., Witzel, T., Zhong, J., Wang, H., Wald, L. L. and Setsompop, K., "Phase-matched virtual coil reconstruction for highly accelerated diffusion echo-planar imaging," *NeuroImage* **194**, 291–302 (2019).
- [15] Manhard, M. K., Bilgic, B., Liao, C., Han, S. H., Witzel, T., Yen, Y. F. and Setsompop, K., "Accelerated whole-brain perfusion imaging using a simultaneous multislice spin-echo and gradient-echo sequence with joint virtual coil reconstruction," *Magnetic Resonance in Medicine* **82**(3), 973-983 (2019).
- [16] Blaimer, M., Guterlet, M., Kellman, P., Breuer, F. A., Köstler, H. and Griswold, M. A., "Virtual coil concept for improved parallel MRI employing conjugate symmetric signals," *Magnetic Resonance in Medicine* **61**(1), 93–102 (2009).
- [17] Setsompop, K., Cohen-Adad, J., Gagoski, B. A., Raij, T., Yendiki, A., Keil, B., Wedeen, V. J. and Wald, L. L., "Improving diffusion MRI using simultaneous multi-slice echo planar imaging," *NeuroImage* **63**(1), 569–580 (2012).
- [18] Setsompop, K., Gagoski, B. A., Polimeni, J. R., Witzel, T., Wedeen, V. J. and Wald, L. L., "Blipped-controlled aliasing in parallel imaging for simultaneous multislice echo planar imaging with reduced g-factor penalty," *Magnetic Resonance in Medicine* **67**(5), 1210–1224 (2012).
- [19] Mani, M., Jacob, M., McKinnon, G., Yang, B., Rutt, B., Kerr, A. and Magnotta, V., "SMS MUSSELS: A Navigator-free Reconstruction for Simultaneous MultiSlice Accelerated MultiShot Diffusion Weighted Imaging" *arXiv preprint. arXiv:1901.01893* (2019).
- [20] Mani, M., Aggarwal, H. K., Magnotta, V. and Jacob, M., "Improved MUSSELS Reconstruction for High Resolution Diffusion Weighted Imaging Using Fast Iterative Re-weighted Least Squares Algorithm," *arXiv preprint arXiv:1906.10178* (2019).
- [21] Setsompop, K., Fan, Q., Stockmann, J., Bilgic, B., Huang, S., Cauley, S. F., Nummenmaa, A., Wang, F., Rathi, Y., Witzel, T. and Wald, L. L., "High-resolution in vivo diffusion imaging of the human brain with generalized slice dithered enhanced resolution: Simultaneous multislice (gSlider-SMS)," *Magnetic Resonance in Medicine* **79**(1), 141–151 (2018).
- [22] Jenkinson, M., Beckmann, C. F., Behrens, T. E. J., Woolrich, M. W. and Smith, S. M., "Fsl," *NeuroImage* **62**(2), 782–790 (2012).
- [23] Andersson, J. L. R., Skare, S. and Ashburner, J., "How to correct susceptibility distortions in spin-echo echo-planar images: Application to diffusion tensor imaging," *NeuroImage* **20**(2), 870–888 (2003).
- [24] Uecker, M., Lai, P., Murphy, M. J., Virtue, P., Elad, M., Pauly, J. M., Vasanawala, S. S. and Lustig, M., "ESPIRiT - An eigenvalue approach to autocalibrating parallel MRI: Where SENSE meets GRAPPA," *Magnetic Resonance in Medicine* **71**(3), 990–1001 (2014).
- [25] Kettinger, A. O., Setsompop, K., Kannengiesser, S. A. R., Breuer, F. A., Vidnyanszky, Z. and Blaimer, M., "Full utilization of conjugate symmetry: combining virtual conjugate coil reconstruction with partial Fourier imaging for g-factor reduction in accelerated MRI," *Magnetic Resonance in Medicine* **82**(3), 1073-1090 (2019).
- [26] Blaimer, M., Jakob, P. M. and Breuer, F. A., "Regularization method for phase-constrained parallel MRI," *Magnetic Resonance in Medicine* **72**(1), 166–171 (2014).
- [27] Kettinger, A. O., Kannengiesser, S. A. R., Breuer, F. A., Vidnyanszky, Z. and Blaimer, M., "Controlling the object phase for g-factor reduction in phase-Constrained parallel MRI using spatially selective RF pulses," *Magnetic Resonance in Medicine* **79**(4), 2113–2125 (2018).
- [28] Hu, Y., Levine, E. G., Tian, Q., Moran, C. J., Wang, X., Taviani, V., Vasanawala, S. S., McNab, J. A., Daniel, B. A. and Hargreaves, B. L., "Motion-robust reconstruction of multishot diffusion-weighted images without phase estimation through locally low-rank regularization," *Magnetic Resonance in Medicine* **81**(2), 1181-1190 (2018).
- [29] Bilgic, B., Chatnuntawe, I., Manhard, M. K., Tian, Q., Liao, C., Iyer, S. S., Cauley, S. F., Huang, S. Y., Polimeni, J. R., Wald, L. L. and Setsompop, K., "Highly accelerated multishot echo planar imaging through synergistic machine learning and joint reconstruction," *Magnetic Resonance in Medicine* **82**(4), 1343-1358 (2019).

- [30] Engström, M. and Skare, S., "Diffusion-weighted 3D multislabs echo planar imaging for high signal-to-noise ratio efficiency and isotropic image resolution," *Magnetic Resonance in Medicine* **70**(6), 1507–1514 (2013).
- [31] Wu, W., Poser, B. A., Douaud, G., Frost, R., In, M.-H., Speck, O., Koopmans, P. J. and Miller, K. L., "High-resolution diffusion MRI at 7T using a three-dimensional multi-slab acquisition," *NeuroImage* **143**, 1–14 (2016).
- [32] Frost, R., Miller, K. L., Tijssen, R. H. N., Porter, D. A. and Jezzard, P., "3D Multi-slab diffusion-weighted readout-segmented EPI with real-time cardiac-reordered k-space acquisition," *Magnetic Resonance in Medicine* **72**(6), 1565–1579 (2014).
- [33] Wu, W., Koopmans, P. J., Frost, R. and Miller, K. L., "Reducing slab boundary artifacts in three-dimensional multislabs diffusion MRI using nonlinear inversion for slab profile encoding (NPEN)," *Magnetic Resonance in Medicine* **76**(4), 1183–1195 (2016).
- [34] Van, A. T., Aksoy, M., Holdsworth, S. J., Kopeinigg, D., Vos, S. B. and Bammer, R., "Slab profile encoding (PEN) for minimizing slab boundary artifact in three-dimensional diffusion-weighted multislabs acquisition," *Magnetic Resonance in Medicine* **73**(2), 605–613 (2015).
- [35] Wang, F., Bilgic, B., Dong, Z., Manhard, M. K., Ohringer, N., Zhao, B., Haskell, M., Cauley, S. F., Fan, Q., Witzel, T., Adalsteinsson, E., Wald, L. L. and Setsompop, K., "Motion-robust sub-millimeter isotropic diffusion imaging through motion corrected generalized slice dithered enhanced resolution (MC-gSlider) acquisition," *Magnetic Resonance in Medicine* **80**(5), 1891–1906 (2018).
- [36] Pauly, J., Nishimura, D., Macovski, A. and Roux, P. Le., "Parameter Relations for the Shinnar-Le Roux Selective Excitation Pulse Design Algorithm," *IEEE Transactions on Medical Imaging* **10**(1), 53–65 (1991).
- [37] Ma, J., Witzel, T., Grissom, W. A. and Setsompop, K., "Minimum peak power root- flipped gSlider-SMS RF pulses for high-resolution in vivo diffusion imaging," *ISMRM*, 0523, Honolulu, HI, USA (2017).
- [38] Eichner, C., Cauley, S. F., Cohen-Adad, J., Möller, H. E., Turner, R., Setsompop, K. and Wald, L. L., "Real diffusion-weighted MRI enabling true signal averaging and increased diffusion contrast," *NeuroImage* **122**, 373–384 (2015).
- [39] Liao, C., Stockmann, J., Tian, Q., Bilgic, B., Manhard, M. K., Wald, L. L. and Setsompop, K., "High-fidelity, high-isotropic resolution diffusion imaging through gSlider acquisition with B1+ & T1 corrections and multi-coil B0 shim array" *arXiv preprint*, arXiv:1811.05473. (2018).
- [40] Liao, C., Wang, K., Cao, X., Li, Y., Wu, D., Ye, H., Ding, Q., He, H. and Zhong, J., "Detection of Lesions in Mesial Temporal Lobe Epilepsy by Using MR Fingerprinting," *Radiology* **288**(3), 804–812 (2018).
- [41] Ma, D., Gulani, V., Seiberlich, N., Liu, K., Sunshine, J. L., Duerk, J. L. and Griswold, M. A., "Magnetic resonance fingerprinting," *Nature* **495**(7440), 187–192 (2013).
- [42] Liao, C., Bilgic, B., Manhard, M. K., Zhao, B., Cao, X., Zhong, J., Wald, L. L. and Setsompop, K., "3D MR fingerprinting with accelerated stack-of-spirals and hybrid sliding-window and GRAPPA reconstruction" *Neuroimage* **162**, 13–22 (2017).
- [43] Cao, X., Ye, H., Liao, C., Li, Q., He, H. and Zhong, J., "Fast 3D brain MR fingerprinting based on multi-axis spiral projection trajectory," *Magnetic Resonance in Medicine* **82**(1), 289–301 (2019).
- [44] Liao, C., Cao, X., Ye, H., Chen, Y., He, H., Chen, S., Ding, Q., Liu, H. and Zhong, J., "Acceleration of MR Fingerprinting with low rank and sparsity constraints," *ISMRM*, 4227, Singapore (2016).
- [45] Tamir, J. I., Uecker, M., Chen, W., Lai, P., Alley, M. T., Vasanawala, S. S. and Lustig, M., "T₂ shuffling: Sharp, multicontrast, volumetric fast spin-echo imaging," *Magnetic Resonance in Medicine* **77**(1), 180–195 (2017).
- [46] Weigel, M., "Extended phase graphs: Dephasing, RF pulses, and echoes - Pure and simple," *Journal of Magnetic Resonance Imaging* **41**(2), 266–295 (2015).
- [47] Bilgic, B., Gagoski, B. A., Cauley, S. F., Fan, A. P., Polimeni, J. R., Grant, P. E., Wald, L. L. and Setsompop, K., "Wave-CAIPI for highly accelerated 3D imaging," *Magnetic Resonance in Medicine* **73**(6), 2152–2162 (2015).
- [48] Gagoski, B. A., Bilgic, B., Eichner, C., Bhat, H., Grant, P. E., Wald, L. L. and Setsompop, K., "RARE/turbo spin echo imaging with simultaneous multislice Wave-CAIPI: RARE/TSE with SMS Wave-CAIPI," *Magnetic Resonance in Medicine* **73**(3), 929–938 (2015).
- [49] Poser, B. A., Bilgic, B., Gagoski, B. A., Uludağ, K., Stenger, V. A., Wald, L. L. and Setsompop, K., "Echo-planar imaging with wave-CAIPI acquisition and reconstruction," *ISMRM*, 1198, Honolulu, HI, USA (2017).
- [50] Cho, J., Park, H., Setsompop, K. and Bilgic, B., "Multi-shot Echo-planar Imaging with Simultaneous MultiSlice Wave-Encoding," *ISMRM*, 4768, Montreal, QC, Canada (2019).
- [51] Zahneisen, B., Aksoy, M., Maclaren, J., Wuerslin, C. and Bammer, R., "Extended hybrid-space SENSE for EPI: Off-resonance and eddy current corrected joint interleaved blip-up/down reconstruction," *NeuroImage* **153**, 97–108 (2017).

- [52] Akçakaya, M., Moeller, S., Weingärtner, S. and Uğurbil, K., “Scan-specific robust artificial-neural-networks for k-space interpolation (RAKI) reconstruction: Database-free deep learning for fast imaging,” *Magnetic Resonance in Medicine* **81**(1), 439–453 (2019).
- [53] Hammernik, K., Klatzer, T., Kobler, E., Recht, M. P., Sodickson, D. K., Pock, T. and Knoll, F., “Learning a variational network for reconstruction of accelerated MRI data,” *Magnetic Resonance in Medicine* **79**(6), 3055–3071 (2018).